JOURNAL OF MATERIALS SCIENCE 31 (1996) 1585–1594

An experimental technique to measure the adhesive strength between inclusions and transparent matrices

T. M. MOWER*
Department of Mechanical Engineering, Massachusetts Institute of Technology, Cambridge, MA 02139, and Lincoln Laboratory, Massachusetts Institute of Technology, Lexington, MA 02173 USA

A. S. ARGON
Department of Mechanical Engineering, Massachusetts Institute of Technology, Cambridge, MA 02139, USA

An experimental method is presented to measure the adhesive strength between spherical inclusions and transparent host matrices. The technique was developed to measure reliably the adhesive strengths between particles and resin matrices. Commonly used adhesion tests possess ill-defined stress concentrations inherent in their design that make them unsuitable for the determination of true adhesive strengths. The procedure developed here involves embedding a sphere of the candidate particle material in the contoured neck portion of a cylindrical epoxy bar (or that of other transparent resin). The decohesion of the sample from the epoxy is observed as the bar is strained in tension. The radial stress at the poles leading to decohesion is then determined by means of a numerical solution of the deformation problem. Adhesive strength data were obtained from a number of epoxy specimens containing particles of Delrin, Nylon, polycarbonate and silica glass, and are presented here and discussed in relation to particle-surface pre-treatments.

1. Introduction

An experimental technique developed to measure the adhesive strength between inclusions and transparent host matrices is presented. The incentive for developing this technique was two-fold. First, it was desired to have a means to measure adhesive strengths between the materials comprising model composite specimens used in a study of crack trapping [1]. Second, although a number of techniques to measure *fibre*–matrix bond strengths and toughnesses have proliferated [2–6], it was recognized that no satisfactory methods have been established to measure reliably the adhesive strengths between particles and resin matrices.

In view of the well-recognized, critical role that adhesive strength plays during the evolution of both crack-tip and crack-flank toughening mechanisms in brittle heterogeneous solids [7–9], it might be expected that good measurements of adhesive strengths exist from prior research focused on this area. On the contrary, investigations of the effect of adhesion upon the mechanical properties of particle-reinforced composites have relied exclusively upon either assumed adhesive characteristics or upon fractographic evidence to provide qualitative rankings of adhesive strength levels as a function of surface preparation. A great deal of research has been focused upon improving the fracture behaviour of brittle polymers, primarily epoxies, through the use of filler particles. A selection of these is listed [10–14]. In those studies in which adhesive strengths were varied, it was found that, depending upon the materials involved, fracture toughness may either increase or decrease as a function of increasing adhesion. In all cases, the adhesive strengths were inferred from examination of fracture surfaces. Although relative adhesion levels are clearly indicated from some particularly enlightening microscopy (e.g. [15]), the effect of adhesive strength upon specific toughening mechanisms and overall fracture toughness should become clearer if quantitative measures of particle/matrix adhesive strength were utilized.

Commonly used techniques of measuring "adhesion", such as lap-shear, butt joint and peel tests are operationally convenient but possess stress concentrations inherent to their design which render them incapable of generating accurate results, representative of true adhesive strengths. The reason for this deficiency is that failures of the standard test joints always proceed through fractures initiated at locations of

* Author to whom all correspondence should be addressed.
"Opinions, interpretations, conclusions, and recommendations are those of the author and are not necessarily endorsed by the United States Air Force."

0022–2461

stress concentration; the joints never fail by uniform stressing across the entire surface. Proper analysis of the mechanics of such fractures will obtain fracture energies of the interface [16], but the "standard" test methods do not provide the magnitude of the intrinsic adhesive strength of the interface.

The experimental technique described here avoids stress concentrations associated with edges by subjecting a spherical particle to a state of triaxial tension. As the applied stress field is steadily increased, the interface between particle and matrix is visually monitored and the magnitude of normal stress which initiates decohesion is determined. Although the stress field surrounding the particle is not purely hydrostatic, the radial stress at the surface is dominant and varies smoothly. Therefore, under the assumption that no initial flaws are present, this level of normal stress is taken to be the "true" adhesive strength exhibited in the tested specimen.

The following sections present the essential background work upon which the technique is based and describes important experimental details, including procedures for preparation of specimens. Photographic records obtained during the testing of a specimen are reproduced, documenting a typical debonding process. The stresses at the particle surfaces just prior to initial decohesion are determined through the use of a finite element analysis. Experimental results are then related and analysed for a series of epoxy specimens containing Delrin, Nylon, polycarbonate and silica-glass spheres. The results are discussed in relation to particle-surface pre-treatments and the apparent roughness of the particle surfaces as revealed in photomicrographs.

2. Background details

The experimental method developed here is a variant of the work of Argon *et al.*, who determined the adhesive strengths of precipitate particles in bars of copper and steel alloys [17]. By tensile straining bars which had been initially machined to a natural neck profile, they induced a state of triaxial stress upon particles contained within the central portions of the specimens. The fractured bars were sectioned and examined to locate the positions of second-phase particles (Fe_3C, Cu–Cr, TiC) which had separated from the bulk metal, nucleating voids. The furthest axial position (from the neck centre) at which particles separated was determined, and the adhesive strength was equated to the radial stress corresponding to this position, which was approximated as [18]

$$\sigma_r \simeq \sigma_y(\bar{\varepsilon}^p) + \sigma \tag{1}$$

where $\sigma_y(\bar{\varepsilon}^p)$ is the local tensile plastic resistance of the (hardening) material and σ is the computed negative pressure, at the site.

An approximate analytical solution for the plasticity problem of the stresses and strains in the neck [19] based upon the work of Bridgman [20] gave the distribution of negative pressure (mean normal stress) along the axis as

$$\sigma_{(r=0)} = \sigma_y\left\{\frac{1}{3} + \ln\left(1 + \frac{a}{2R}\right) - 2\ln\left[1 + \frac{z^2}{a(a + 2R)}\right]\right\} \tag{2}$$

where z is the axial position from the centre, a is the minimum section radius and R is the minimum radius of the neck profile. This expression indicates that σ is proportional to the flow stress, so that a state of pure hydrostatic tension may be expected to develop only after plastic strains are produced in much of the neck. In addition, Argon *et al.* indicate that Equation 2 is valid only for axial positions near the necked region, where the profile is concave outwards [17]. For regions located further away along the axis, numerical computations [19] based upon the methods of Needleman [21] provided the magnitudes of σ as a function of plastic strain and axial position.

To determine a mathematical representation of the natural neck profile, many ductile copper bars were necked and carefully measured [22]. An empirical fit to these measurements was given as [19]

$$r = a_o\left(1 - v\left\{\left[1 + \frac{1}{(z/a_o)^2 + v^2}\right]^{1/2} - 1\right\}\right) \tag{3}$$

with

$$v \equiv \frac{(a/a_o)[2 - (a/a_o)]}{2[1 - (a/a_o)]} \tag{4}$$

where a is the radius of the central section and a_o is the radius at a great distance from the neck in the uniform region of the bar. By straining specimens with profiles machined according to this expression, a state of triaxial stress can be generated within the neck region to explore decohesion and cavitation phenomena.

With the adaptation of this technique to glassy polymer matrices, it was anticipated that the adhesive strength between the particles and the matrix might be reached prior to any significant development of plastic strains. Therefore, the use of the Bridgman solution for stress at the neck centre would not be fully valid. An alternative might be to use an elastic solution developed by Neuber for circumferentially grooved bars, but that solution was based upon a profile with a constant radius of curvature [23]. An additional complexity arises, due to the presence of an elastic stress concentration, if the particles included in the neck have a much higher modulus than the polymer from which the neck is fabricated. Consequently, a finite element analysis was employed to determine the state of stress in the natural neck specimens used here, where, moreover, no approximation was made about the initial state of the material.

The overall strategy adopted here entailed the casting of a spherical particle of a candidate material at the centre of a solid bar of epoxy, which was then machined with a numerically controlled lathe to the

profile given by Equation 3. The neck was then strained in tension, while an image of the particle surface was continuously recorded. The adhesive strength of the particle/matrix interface was then determined, using the applied load which caused debonding to occur. The critical level of the radial stresses were obtained from the finite element solution.

3. Experimental procedure

3.1. Fabrication of specimens

The neck specimens were cast from a typical DGEBA epoxy (Shell EPON 815) cured with a difunctional polyamide (V-40) at a mix ratio of 3:1. The particles which were used in these adhesive strength measurements to epoxy were Delrin, Nylon, polycarbonate and soda-lime (silica) glass. The polymers were obtained as 3.17 mm diameter spheres with a sphericity (diameter tolerance) better than 0.5%; the spherical silica-glass particles had a nominal diameter of 2.8 mm.

The most difficult aspect of specimen fabrication was the placement of the spherical particles in the centre, both radially and longitudinally, of a solid bar of epoxy without creating a weak mechanical interface between the two sections of the epoxy, which would cause premature parting. The successful scheme that was developed utilized the following procedures. The moulds used to cast the epoxy rods were thin-walled (1.5 mm) tubes of polymethyl methacrylate (PMMA), 51 mm outside diameter and approximately 35 cm long. Because the glass transition temperature, T_g, of PMMA is about 110 °C, a maximum curing temperature 100 °C was used. The T_g of the epoxy specimens cast into the tubes was 72 °C (determined by means of differential scanning calorimetry). Aluminium plugs were coated with a release agent and then inserted into the bottom of the PMMA tubes. Epoxy resin was mixed with curing agent, degassed, and poured into the tubes up to the half-length of the desired solid rods. The half-filled tubes were placed in a tall vacuum chamber to degas the contents once again. After all visible bubbles were evacuated, the vcauum was removed and sufficient time was allowed to cause the surface deformation resistance to increase (through gelation) enough to support a sphere placed upon the surface.

At this point, one of the candidate spheres (properly solvent-cleaned, dried and, in some cases, surface-modified) was placed upon the conical tip of a Teflon positioning jig having a through-hole drilled along the axis of revolution. Suction was then applied to the jig to hold the particle in place, as shown schematically in Fig. 1. A tiny drop of freshly mixed, degassed epoxy was then placed on the sphere. The positioning jig with sphere in place was then inserted into a half-filled mould and slowly pushed in until the sphere was partially indented into the epoxy surface. The suction was then removed from the jig, which was extracted after the stability of the position of the sphere was established. A further period of time was allowed for gelation of the hemispherical bond, but not enough time to allow vitrification; too much curing at this

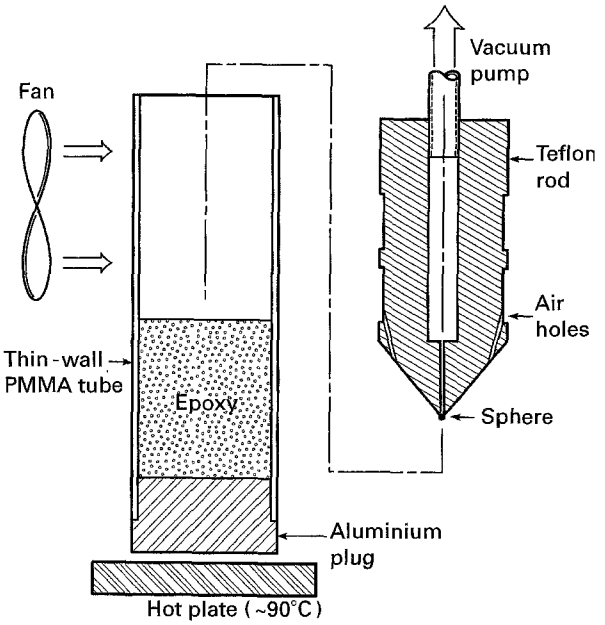

Figure 1 Schematic drawing of procedure used to cast spheres in the centre of epoxy rods for adhesive-strength neck specimens.

stage was found to result in an interface of reduced strength between halves of the finished solid. Finally, the moulds were filled to within about 3 cm of the top and then evacuated until all bubbles were removed (or at least, removed from regions near the sphere).

To prevent shrinkage voids from forming during the first curing stage of the epoxy rods, a vertical temperature gradient was established so that curing would progress from the constrained lower sections upwards. To accomplish this, the filled moulds were placed upon a laboratory hot plate maintained at about 90 °C and a fan was positioned to blow cool air across the upper halves of the moulds. Following such a controlled temperature-gradient curing process for 12 h, the specimens were kept at room temperature for another 24 h so that nearly all room-temperature reaction could be completed. They were then placed in a programmable oven, which controlled the post-cure temperature to a maximum of 100 °C and slowly cooled the specimens down to room temperature again. The moulds were then cracked, pried and peeled apart from the finished epoxy rods.

In the next step of fabrication, the rods were machined to a total length of 25.4 cm with the particle located exactly in the centre. Each rod was then machined on a numerically controlled lathe, which had been programmed from data produced by Equation 3. The radius of the central neck section, $a = 22$ mm, was prescribed as one-half the radius, a_0, of the distant end to be held by grips. A plot of this profile is shown in Fig. 2, which shows the bevelled collars machined at the specimen ends to provide the gripping surfaces for applying tensile loading. After the contours were machined, each specimen was again mounted in a lathe for final finishing. Successively finer grits of wet/dry sandpaper and water were used to smooth the neck surfaces. Final polishing as accomplished with alumina paste and cloths. A few fine scratches were allowed to remain over most of the surface areas; near

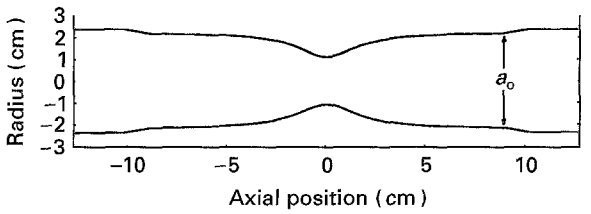

Figure 2 Profile from Equation 3, with $a/a_o = 0.5$, used to machine neck specimens with numerically controlled lathe.

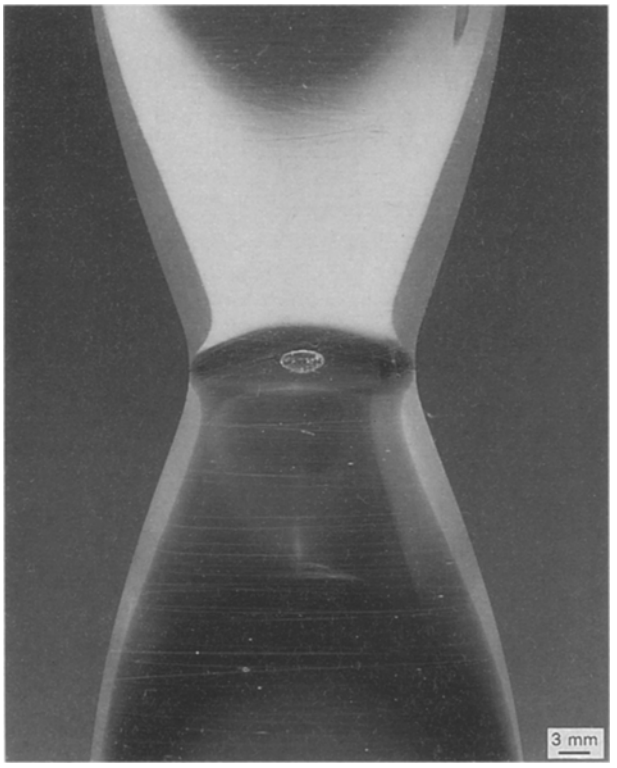

Figure 3 Close-up of finished neck specimen with glass particle. The particle appears distorted by the concave free surface.

the central neck region, all scratches were removed to reduce the chance of fracture due to flaws on the highly stressed surface during testing. A photograph of the central portion of a specimen containing a silica-glass is reproduced in Fig. 3.

3.2. Testing procedure

To subject the necked adhesive strength specimens to tension, special grips were machined from aluminium blocks. Each grip consisted of two mating halves, bolted together and bored out to accommodate the contour of the specimen ends shown in Fig. 2. A bevelled surface at the bottom of the grips, matching the tapered shoulder of specimens, provided the bearing surface for loading. Large (31 mm diameter) pins connected the grips to a standard testing machine.

The necked specimens were strained in tension at room temperature with a grip-displacement rate of $5\,\text{mm}\,\text{min}^{-1}$. This translates to a nominal applied strain rate of $\dot{\varepsilon} \sim 3.3 \times 10^{-4}\,\text{s}^{-1}$, based upon uniform deformation of the entire specimen length. Owing to the non-uniform diameter of the specimens, the actual strain rate in the neck region was about an order of magnitude higher (indicated by the finite element simulations). Load data were measured with a 45 kN load cell and recorded on a time-based strip chart recorder. During the loading of each specimen, a 16 mm movie of the sphere was recorded at a rate of 24 frames per second. Lighting was provided by a fibre optic light source. The start of each film segment was synchronized with locations on the strip chart, so that correlation of the film rate and chart speed would provide the magnitude of applied load corresponding to recorded debonding events.

3.3. Examples of debonding images

Debonding events in necked specimens containing particles with low to moderate adhesive strength to epoxy, such as Delrin and Nylon, or PC and silica-glass particles with release-coated surfaces, could usually be observed both in real time and when viewing the recorded films. Debonding always initiated at either one or both poles of the sphere. In cases with very low adhesive strength (Delrin), debonding continued along the interface until at least an entire hemisphere was debonded and little traction could be applied to the sphere. In cases with moderate adhesive strength and interfacial toughness, debonding advanced slowly along the interface until conditions became favourable for the crack to kink into the epoxy. At this point, the critical crack size for the current local stress level had invariably been reached for the epoxy, and rapid fracture ensued across the neck.

A sequence of images recorded during the debonding of a Delrin particle is shown in Fig. 4. In these images, the debonding is manifested by dark patches growing on the surface and by bright reflection of light from the new surfaces. In the example shown here, the debonding of the Delrin sphere proceeded initially from the south pole, but was joined by debonding from the north pole prior to the unloading of the neck specimen. Nylon spheres and PC or silica-glass spheres which had been treated with a release agent also debonded slowly enough to record the process continuously on film.

In cases of extremely well-bonded particles, such as silica-glass or polycarbonate, debonding occurred at such a high applied load that the critical flaw size (corresponding to the applied stress and the fracture toughness of the epoxy through the relation $\pi a_{cr} = (K_{IC}\pi/2\sigma_1)^2$, which is derived for a three-dimensional penny-shaped crack [24]) for the epoxy matrix was quickly reached and rapid fracture of the specimen ensued. In these cases, no satisfactory debonding images were recorded (due to the slow frame rate of filming at 24 f.p.s.), and the debonding load was determined from the peak load of specimen failure.

A typical example of a fracture resulting from the debonding of a glass sphere in a necked adhesive strength specimen under high stress is reproduced in Fig. 5. The smallest circular area seen in the centre of this photograph is the debonded region, where the crack travelled along the interface before kinking into the epoxy. When the crack first began propagating in

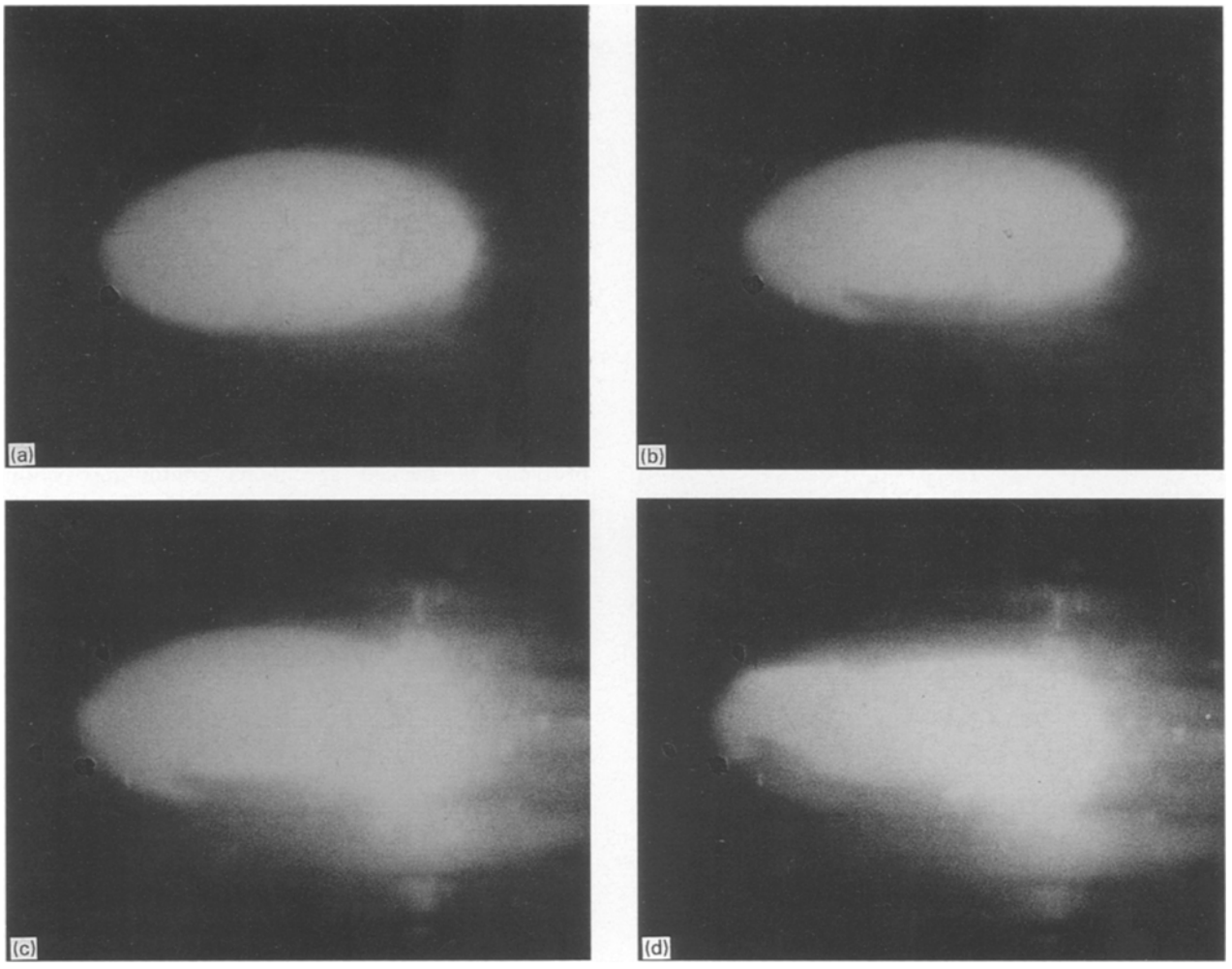

Figure 4 Sequence (a–d) of 16 mm images recorded during debonding of a Delrin sphere in a necked adhesive-strength specimen.

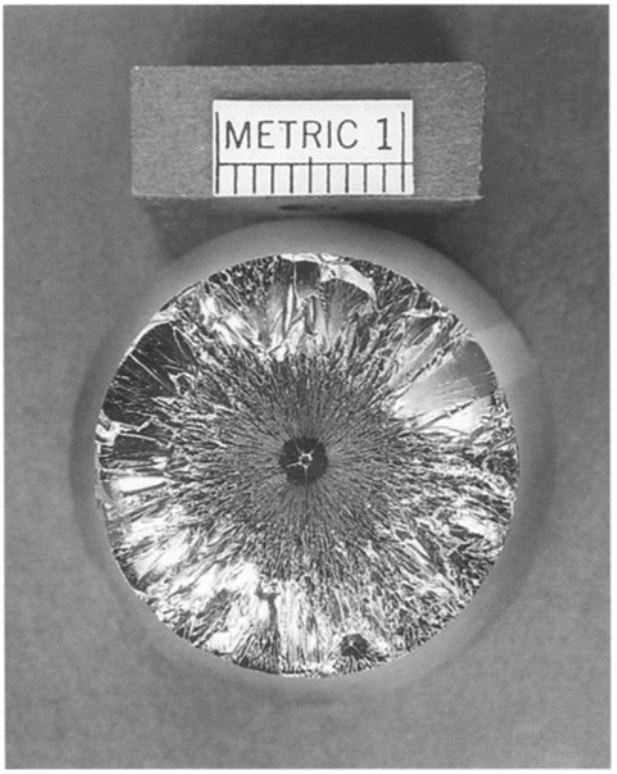

Figure 5 Typical radial fracture initiated by debonding at the pole of a glass sphere. The crack travelled along the interface a short distance, kinked into the epoxy and propagated in three distinct modes (discussed in text). The particle remains below the exposed surface.

the epoxy, it travelled at a relatively "low" velocity (less than 100 $m\,s^{-1}$), leaving a smooth surface. (Directly beneath this area, and having a similar diameter, is the particle remaining in the epoxy.) The crack velocity then approached its limit of about one-third the elastic wave speed, $(E/\rho)^{1/2}$, and began creating a rougher fracture surface. This surface extends to about one-half the specimen radius, at which point the fracture surface becomes grossly rough, with large chips missing. The location of this transition corresponds well to the meeting of the crack front with the reflection from the free surface of the original stress wave created by the fracture initiation. Similar fracture surfaces were created by the debonding of glass spheres in other necked specimens.

An example of the fracture surface of a specimen having no relation to debonding is shown in Fig. 6. The figure shows clearly that the fracture origin of this necked specimen was on the free surface, perhaps at a scratch that had not been removed by polishing or from a nick created in subsequent handling. Clearly, such failures, resulting in no useful data, were ignored.

4. Finite element stress analysis

4.1. Elastic solution

A numerical solution for the stresses resulting from deformation of the necked adhesive strength specimens was obtained with the commercial finite element

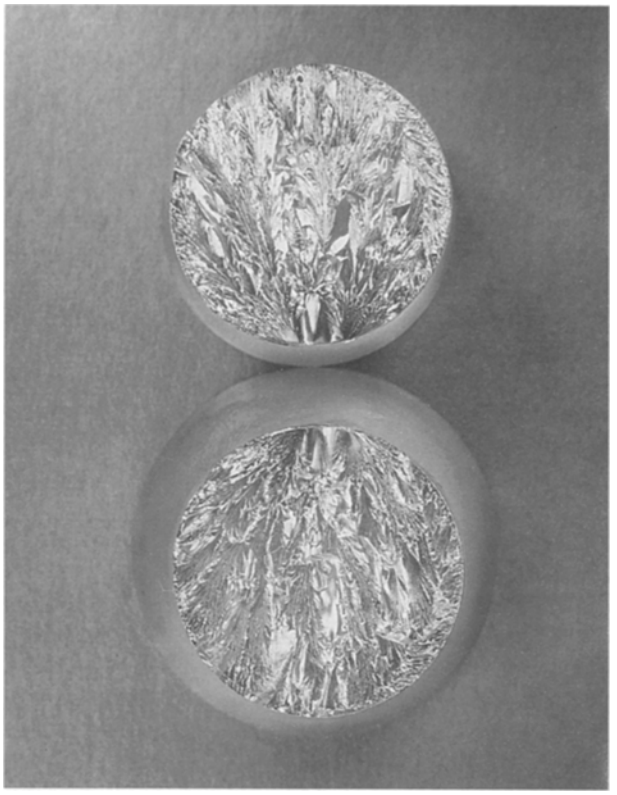

Figure 6 Typical fracture initiated by surface defect.

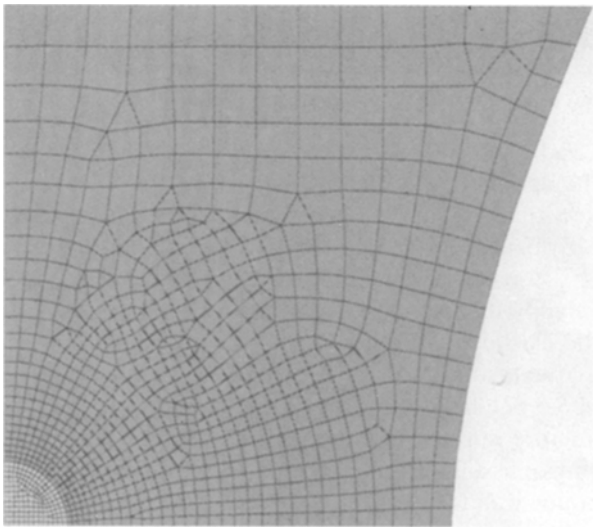

Figure 7 Meshing used to model the central portion of neck specimens. Elements shown here (except those representing the sphere) were assigned a bi-linear hardening behaviour. The remainder of the specimen (not shown) was incorporated into an elastic super-element.

program, ANSYS [25]. The necked specimen was modelled with eight-noded, isoparametric, quadrilateral elements, which provide better solutions to problems where stress gradients or curved surfaces are present than do constant-stress, four-noded elements. Because the neck is a solid of revolution, it was represented by axisymmetric finite elements, which reduce the problem to two-dimensions (one layer thick). In addition, the neck is symmetric about its centre section. Therefore, boundary conditions of symmetry were applied to the longitudinal (y) axis and to the centre radial (x) axis. The contoured free surfaces were treated as traction free. Load was applied to the end section corresponding to the grip position. The meshing density as adjusted so that increasingly finer elements were employed as the section radius decreased. The central region, shown in Fig. 7, was finely divided with 786 elements, exclusive of the sphere. The remainder of the neck was incorporated into an elastic super-element, greatly reducing computation times in the plastic solutions which required iterative computations. The sphere itself was modelled with 154 elements having edge lengths equal to about 8% of the sphere radius.

An elastic finite element solution to the deformation problem of necked specimens containing Nylon spheres showed that, at the maximum load at debonding which was experimentally recorded, the equivalent stress, $\bar{\sigma}$, everywhere remained below the rate-dependent yield stresses of both the epoxy and the Nylon. Consequently, this single solution furnished the magnitudes of stresses which would result from any other (lower) load. In this elastic analysis, Young's modulus of the Nylon was taken (from auxiliary measurements) to be $E = 2.8$ GPa. Poisson's ratio for the Nylon was assumed to be $\nu = 0.34$; for the epoxy, a value of $\nu = 0.36$ was assumed. Young's modulus for the epoxy at the approximate strain rate generated during testing of the necks was taken (also from auxiliary measurements) as $E = 2.2$ GPa. Radial stresses computed within and immediately adjacent to the Nylon sphere were, as expected, continuous across the interface and maximum at the pole.

4.2. Elastic–plastic solution

Analysis of neck specimens containing particles with relatively high adhesive strengths (PC and silica-glass) required the incorporation of a non-linear stress–strain relation for the epoxy, representing its plastic response. The non-linear numerical solution was implemented by applying the load in 0.85 MPa increments of stress at the end sections. Within each stress increment, iterative solutions were computed until the plastic strain increment converged to less than 1% of the current elastic strain. The measured true stress–strain behaviour of the epoxy was represented by a yield stress of $\sigma_y \approx 60$ MPa followed with bi-linear hardening, at rates of $d\sigma/d\varepsilon = 4$ and 40 MPa. Elastic properties assigned for the PC spheres were $E = 2.2$ GPa and $\nu = 0.35$; for the silica-glass spheres, $E = 69.5$ GPa and $\nu = 0.24$.

At the highest experimentally applied stress level (17 MPa at the end sections) sustained by necks containing PC spheres, the finite element (FE) analysis predicted that a region of plastic flow had spread inward from the necked surface to about half of the neck radius, and still no yielding occurred near the sphere. In the case of specimens containing silica-glass particles, FE analysis showed that the maximum applied stress developed $\bar{\sigma}$ levels exceeding the yield stress of the epoxy in three small regions: one at the neck surface, on directly above the glass particle and

the other on the particle surface at a latitude of about 45°.

4.3. Stresses at particle surfaces

In naturally necked cylindrical bars, hydrostatic tension, σ, develops as a consequence of non-uniform strain hardening and deformed geometry. In bars machined to a natural neck profile, the hardness of the material is uniform at the onset of testing, but the contoured shape rapidly concentrates strain in the central region of the neck in a manner that generates triaxial tension [19], which varies smoothly and has no discontinuities. Plotted in Fig. 8 are computed values of σ_r at the surface of the spheres, resulting from the maximum applied stress recorded experimentally for debonding of each type of sphere material. The magnitudes of σ_r remain relatively constant (within $\sim 15\%$ of the peak values at the pole) in each case as θ varies from 0 to 20°.

Because there is no sharply localized stress concentration at the site where decohesion originates (invariably at the pole), the adhesive strength of the bond between a sphere and the neck material can be characterized well by the magnitude of polar radial stress which causes initial decohesion to occur. Values of σ_r at the poles, computed by FE analysis for the three types of spheres are plotted in Fig. 9 as a function of increasing tensile stress applied to the ends of the specimen. These data were used to determine adhesive bond strengths from experimentally observed decohesion loads.

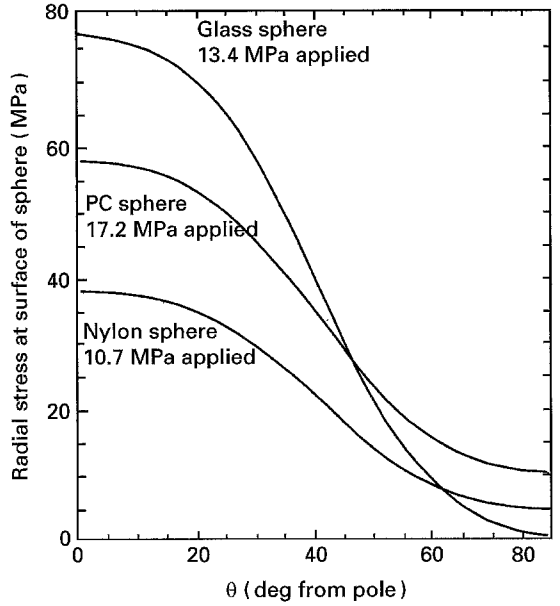

Figure 8 Radial stress at the surface of spheres in the necked region of specimens subjected to the stresses indicated. From FE analysis.

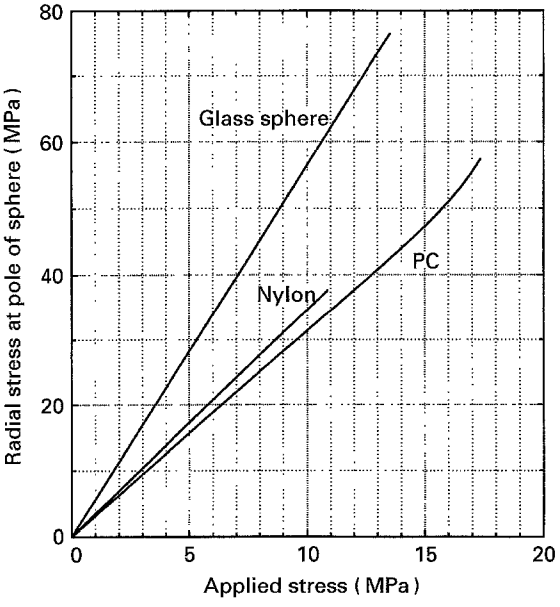

Figure 9 Radial stress at the pole of spheres in necked adhesive-strength specimens as a function of increasing stress applied to the ends of the specimens. From FE analysis.

5. Determination of adhesive strengths

During testing of each of the necked adhesive-strength specimens, initial debonding at a pole of the included sphere occurred when the radial stress across the interface exceeded the strength of the bond, and resulted in the formation of a three-dimensional interfacial crack. Subsequent propagation of this crack proceeded typically in one of two ways. With spheres having low adhesive strengths to epoxy, initial debonding was followed by relatively slow advance of the interfacial crack towards the equator, until the crack kinked into the epoxy and rapid fracture of the necked section resulted. Debonding of sphere surfaces with greater adhesive strengths to epoxy occurred at such high loads that the resulting interfacial cracks immediately reached the critical flaw size for the epoxy, so that the debonding process could not be temporally separated from the final fracture process.

The applied stresses which initiated debonding were combined with the results of the FE analysis to determine the radial stress acting upon each sphere/epoxy interface at the moment when debonding occurred. The residual stresses, resulting from the differential thermal contractions between the sphere materials and the epoxy necks during cooling after the post-curing of the epoxy, were accounted for in the following manner. The residual radial stresses were computed analytically for each sphere material using expressions available in the literature [26] and measurements of the differential thermal strains which were established over the temperature interval from the glass transition temperature for the epoxy, $T_g = 72\,^{\circ}C$, to room temperature. The individual thermal strains of the epoxy and the spheres were measured with a thermomechanical analyser; these measurements and the computation of residual stresses are discussed in detail elsewhere [1]. Using the elastic constants which were stated earlier, the residual stresses computed for each sphere/epoxy combination are: Nylon, $\sigma_r^{res} \approx 3$; PC, $\sigma_r^{res} \approx -3$; and silica-glass, $\sigma_r^{res} \approx -10$ MPa. Only very slight relaxation of these stresses will have occurred during the room-temperature storage of specimens prior to testing [27, 28]. Therefore, the computed residual stress values were

added directly to the applied radial stresses to arrive at the adhesive strength data which are summarized in Table I. (The elastic and thermal properties of Delrin were assumed to be similar to those of Nylon.)

6. Discussion

The data in Table I indicate that the measured adhesive strength of as-received (solvent-cleaned) Delrin (acetal) to epoxy is approximately 15 MPa. This low level of adhesive strength is consistent with the well-known low surface energy of acetal.

The data indicate that the adhesive strength of the as-received Nylon to epoxy is approximately twice that of Delrin, despite the smooth, "smeared over" appearance of the surface of the Nylon spheres in the as-received condition, as indicated by the scanning electron micrographs shown in Fig. 10. Following a method reported by Shields [29], improvement of the adhesive strength between Nylon and epoxy was attempted by first etching the Nylon with an acid/potassiumpermanganate solution and then treating the etched surface with a resorcinol–formaldehyde primer. Photographs of a typical etched Nylon surface are reproduced in Fig. 11. Clearly, the aggressive acid/permanganate etching process created many tiny oles and pits, which may improve adhesion through mechanical interlocking [30], but surface cracks have been introduced whose effect upon adhesive strength is likely to be detrimental. Indeed, the data indicate that the etched Nylon surface has a lower adhesive strength to epoxy than the as-received Nylon. Application of the primer to etched Nylon surfaces created a patchwork of primer material, filling the surface pits and cracks with fibrous and dendritic-looking growths as shown in the micrographs of Fig. 12. These structures appear similar to copper oxide growths on anodized copper surfaces which demonstrated enhanced adhesion [31]. As indicated by the data in Table I, priming the etched Nylon surfaces with resorcinol–formaldehyde restored the mean measured adhesive strength to the level exhibited by as-received specimens.

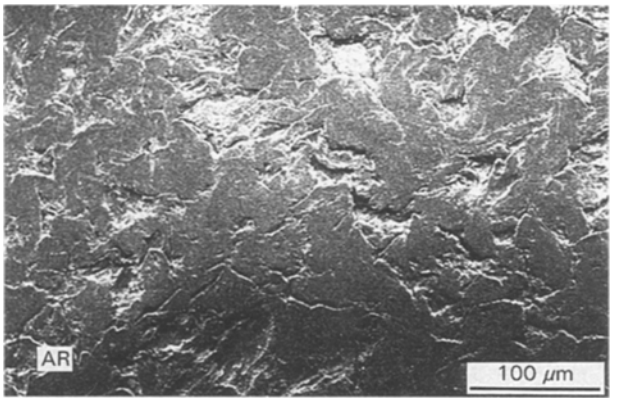

Figure 10 Scanning electron micrograph of the surface of a Nylon sphere, as-received.

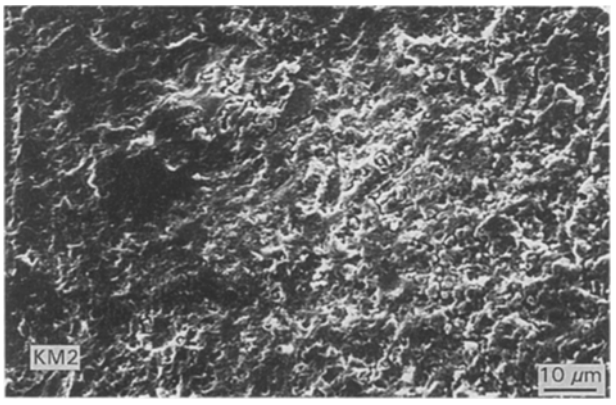

Figure 11 Scanning electron micrograph of surface of Nylon sphere, etched with $KMNO_4$–H_2SO_4 at 90 °C for 5 min and ultrasonically cleaned in isopropanol.

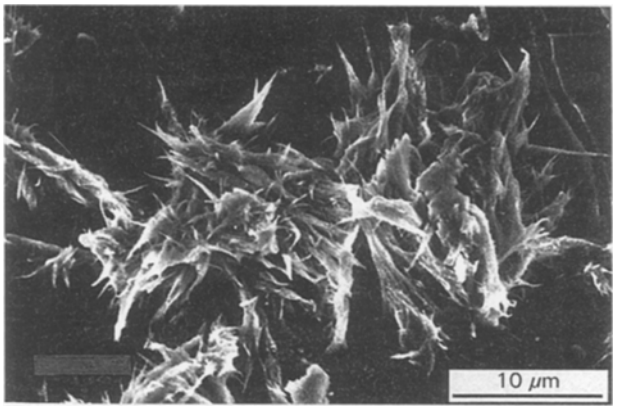

Figure 12 Scanning electron micrograph showing growth of fibrous structures on etched and resorcinol–formaldehyde primed surface of a Nylon sphere.

In the case of specimens containing as-received (solvent-cleaned) PC spheres, no debonding was observed; fractures in these specimens initiated in the epoxy near the equator of spheres and rapidly spread across the neck sections, fracturing the PC spheres in the process. A typical example of this mode of specimen failure is shown in the photographs of Fig. 13. The fracture surface shown in the light micrograph indicates the dynamic, brittle mode of fracture through the epoxy surrounding the PC sphere. (The void in the centre of the PC sphere was formed during its manufacture.) The scanning electron micrograph reveals characteristic hackle marks in the epoxy leading back to the origin of the fracture, at the sphere/epoxy interface near the equator. Because debonding of the as-received PC spheres did not occur, the radial stress generated at the particle poles as a result of the maximum applied loads is a measure of a lower bound to the adhesive strength between PC and epoxy.

The lower bound to the adhesive strength of epoxy to polycarbonate is established by the data shown here as approximately 54 MPa. This very high level of adhesion, for a resin to a low surface-energy polymer, certainly results, in part, from the rough, as-received surface of the PC spheres. Fig. 14 contains SEM images of the surface of a PC sphere in the as-received condition. These images reveals a uniformly rough surface with ubiquitous ledges and crevices, providing extensive opportunities for mechanical interlocking of

TABLE I Measured adhesive strengths of listed materials to epoxy

Material	Surface treatment	Adhesive strengths (MPa)	*Mean* (S.D.)
Derlin	Solvent cleaned	14.7; 15.5; 16.6	15.6 (0.9)
Nylon	Solvent cleaned	24.2; 28.2; 34.3; 40.1	30.7 (6.9)
	$KMNO_4$ etched	17.1; 19.1; 22.1; 24.2	20.6 (3.1)
	Etched; resorcinol–formaldehyde Primer	26.1; 28.2; 29.8; 30.2 31.8; 33.6; 34.8; 38.2	31.6 (3.8)
Glass	Solvent cleaned	55.3; 59.4; 63.5; 66.1	61.1 (4.7)
	Release coated	44.5; 50.8; 31.2 (2 coats)	
	Silane coated	46.0; 50.1; 53.4	49.8 (3.7)
PC	Solvent cleaned	> 49.6; > 49.6; > 53.5; > 54.2	> 54
	Release coated	22.2; 27.8; 30.9; 31.3	28.0 (4.2)
	Released (2 coats)	19.5; 21.0; 22.6; 24.5	21.9 (2.1)

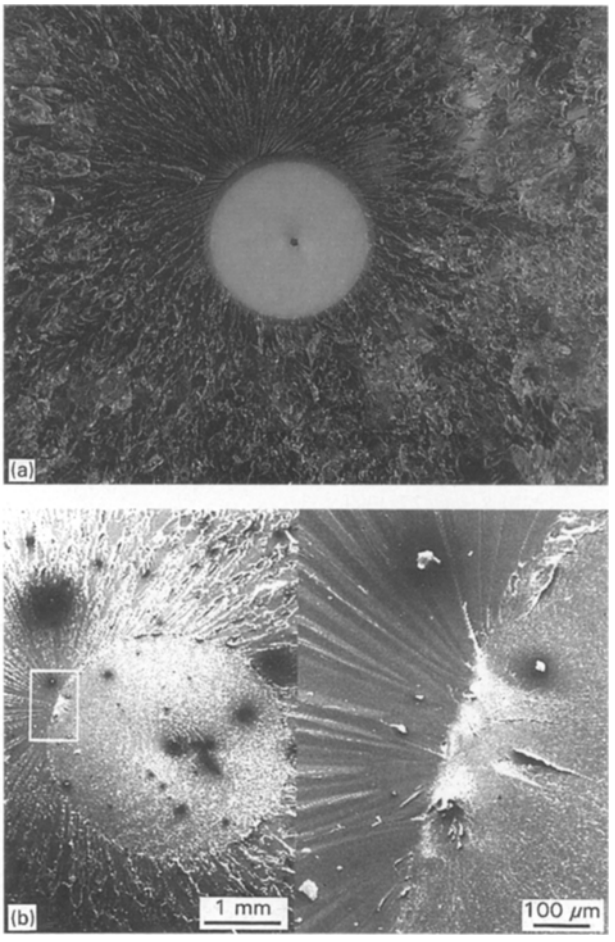

Figure 13 Typical failure surface of necked specimen containing PC sphere. Debonding did not occur: failure resulted from fracture originating within epoxy, indicated by hackle marks leading back to the origin at the equatorial surface of the sphere.

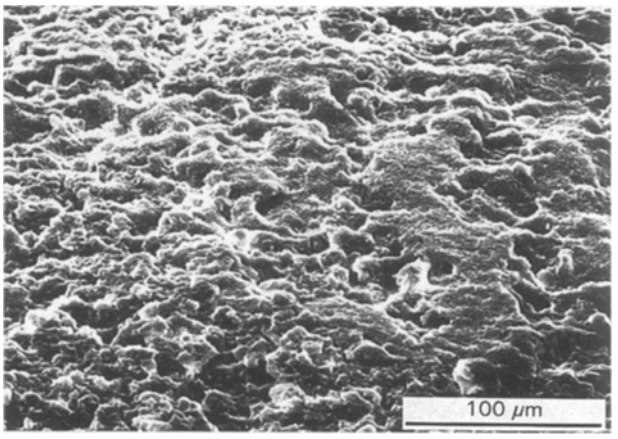

Figure 14 Scanning electron micrograph of the surface of a PC sphere, showing extensive, uniformly distributed three-dimensional features which enhance adhesive strength through mechanical interlocking.

adhesive resins. The high adhesive strength of PC to epoxy could readily be reduced through the application of a surface release agent. Application of one coat of release agent (Free-Kote) reduced the PC/epoxy adhesive strength to a level comparable to the Nylon/epoxy adhesive strength. Additional coats of release agent will, of course, further reduce the adhesive strength.

Silica-glass particles exhibited very high adhesive strengths to the epoxy resin. In the as-received condition, the mean measured adhesive strength slightly exceeded the nominal yield stress of the epoxy (~ 60 MPa). Such a high level of adhesion is reached in spite of the smooth surface of the glass particles, demonstrated by the micrograph in Fig. 15a, due to strong intermolecular forces of attraction resulting from the large polar component of surface free energy possessed by the silica [32]. Application of release agent caused a reduction in the adhesive strength by about 10 MPa per coat of release. Treatment of the glass particles with a 1% silane (gamma-amino., Union Carbide A-1100) aqueous/isopropyl solution did not increase the adhesive strength to epoxy, but reduced it instead, perhaps due to the formation of a weak interlayer.

Debonding at the polar cap of spheres in the necked specimens introduces a circular interfacial crack which is initially normal to the axis of symmetry. If the toughness of the interface, $\mathcal{G}_c^{int}$, is less than the toughness of the matrix, $\mathcal{G}_{Ic}^{mat}$, the crack will propagate along the interface. As the crack advances circumferentially towards the equator, the stress intensity, K_I^{int}, along the interface will diminish due to the change in orientation of the crack tip with respect to the applied stress field, while K_I^{mat} will increase due to the increasing effective crack radius, a (normal to the cylinder axis). When conditions become more favourable for fracture through the neck section than for

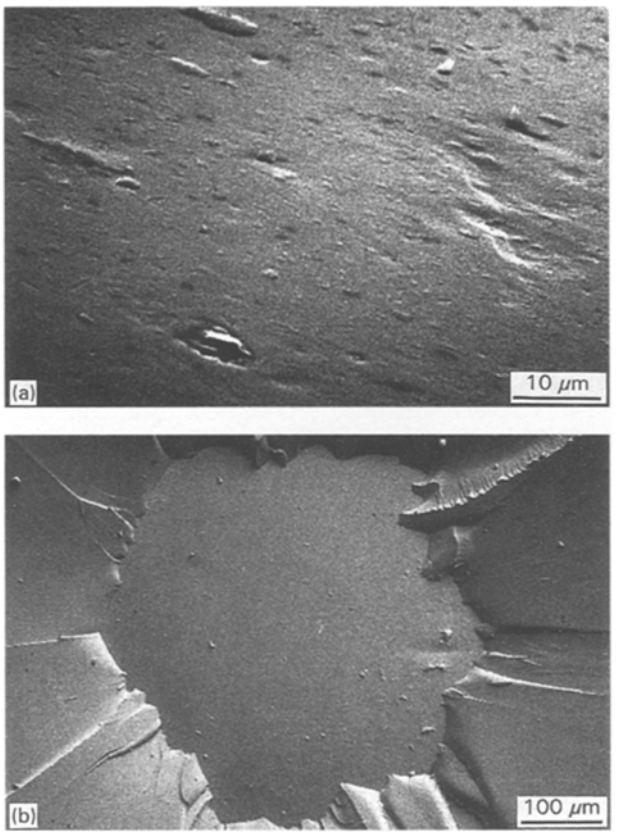

Figure 15(a) Scanning electron micrograph of debonded surface of silica-glass sphere. The surface is smooth, though pits in glass and attached shards of epoxy are apparent. (b) Scanning electron micrograph of a typical fracture surface resulting from debonding of a silica-glass sphere, demonstrating sharp transition of the crack path from the interface to the bulk epoxy.

continued fracture along the interface, the crack will "kink" into the epoxy neck. The angular position, θ, of the crack-path kinking from the interface into the matrix can be obtained from micrographs of exposed spherical surfaces, such as that shown in Fig. 15b. The toughness of the spherical interface can then be determined, knowing $\mathscr{G}_{\mathrm{Ic}}^{\mathrm{mat}}$ and θ, from solutions of stress intensity factors for spherical cracks [33]. This extension of the adhesive strength measurements related here is presented elsewhere [34].

7. Conclusion

An experimental technique has been presented to enable the measurement of true adhesive strengths between particles and transparent host matrices, by subjecting a spherical particle to a state of smoothly varying triaxial stress. Adhesive strength data were obtained from a number of epoxy specimens containing particles of Delrin, Nylon, polycarbonate and silica glass. The measured adhesive strengths of these materials to epoxy resin were discussed as a function of various surface pre-treatments and the surface roughness as indicated by microscopy. It is suggested that the adhesive strength measurement technique presented here could be applied to future studies of toughening mechanisms in composites containing particles, enabling the effects of adhesion to be more thoroughly understood.

Acknowledgements

Support for this work was provided by the Department of the Air Force and is gratefully acknowledged. We thank Michael Imbeault of Lincoln Laboratory, for recording photographic images of the debonding events and the subsequent fracture surfaces. We thank Bill DiNatale, also of Lincoln Laboratory, for the extensive SEM microscopy which he provided. The generous provision of epoxy by the Shell Chemical Co. is appreciated.

References

1 T. M. MOWER and A. S. ARGON, *Mech. Mater.*, **19** (1995) 343.
2 L. J. BROUTMAN, in "Interfaces in Composites", ASTM STP *452* (American Society for Testing and Materials, Philadelphia, PA, 1969) p. 27.
3 C. C. CHAMIS, in "Composite Materials", Vol. 2, "Interfaces in Polymer Matrix Composites", edited by L. J. Broutman and R. H. Krock (Academic Press, New York, 1974), pp. 31–77.
4 C. ATKINSON, J. AVILA, E. BETZ and R. E. SMELSER, *J. Mech. Phys. Solids* **30** (1982) 97.
5 J. L. KOENIG and H. EMADIPOUR, *Polym. Compos.* **6** (1985) 142.
6 N. IKUTA, Z. MAEKAWA, H. HAMADA, M. ICHIHASHI and E. NISHIO, *J. Mater. Sci.* **26** (1991) 4663.
7 A. S. KENYON, *J. Coll. Interface Sci.* **27** (1968) 761.
8 M. R. PIGGOT, *Polym. Compos.* **3** (1982) 179.
9 L. T. DRZAL and M. MADHUKAR, *J. Mater. Sci.* **28** (1993) 569.
10 L. J. BROUTMAN and S. SAHU, *Mater. Sci. Eng.* **8** (1971) 98.
11 A. J. KINLOCH, D. L. MAXWELL and R. J. YOUNG, *J. Mater. Sci.* **20** (1985) 4169.
12 W. J. CANTWELL, J. W. SMITH, H. H. KAUSCH and T. KAISER, *ibid.* **25** (1990) 633.
13 J. SPANOUDAKIS and R. J. YOUNG, *ibid.* **19** (1984) 487.
14 A. C. MOLONEY, H. H. KAUSCH and H. R. STIEGER, *ibid.* **18** (1984) 208.
15 J. D. MILLER, H. ISHIDA and F. H. MAURER, *ibid.* **24** (1989) 2555.
16 A. N. GENT and C. W. LIN, *J. Adhes.* **30** (1989) 1.
17 A. S. ARGON and J. IM, *Metall. Trans. A* **6** (1975) 839.
18 A. S. ARGON, J. IM and R. SAFOGLU, *ibid.* **6** (1975) 825.
19 A. S. ARGON, J. IM and A. NEEDLEMAN, *ibid.* **6** (1975) 815.
20 P. W. BRIDGMAN, "Studies in Large Plastic Flow and Fracture" (McGraw-Hill, New York, 1952).
21 A. NEEDLEMAN, *J. Mech. Phys. Solids* **20** (1972) 11.
22 J. IM, SM thesis, MIT (1971).
23 H. NEUBER, "Theory of Notch Stresses" (Edwards, Ann Arbor, MI, 1946), pp. 849.
24 J. G. WILLIAMS, "Stress Analysis of Polymers" (Ellis Horwood, New York, 1980) p. 323.
25 ANSYS©, Rev. 4.4A, (Swanson Analysis Systems, Houston, PA 1990).
26 J. SELSING, *J. Am. Ceram. Soc.* **44** (1961) 419.
27 P. S. THEOCARIS, *Rheol. Acta* **6** (2) (1967) 246.
28 M. E. BOYCE, A. S. ARGON and D. M. PARKS, *Polymer* **28** (1987) 1680.
29 J. SHIELDS, Sira Institute Report, **R500**, Kent, UK, (1972).
30 A. J. KINLOCH, *J. Mater. Sci.* **15** (1980) 2141.
31 J. R. G. EVANS and D. E. PACKHAM, *J. Adhes.* **10** (1979) 177.
32 A. J. KINLOCH, "Adhesion and Adhesives" (Chapman and Hall, London, 1987), p. 33.
33 G. XU and M. ORTIZ, *Int. J. Num. Meth. Eng.*, **36** (21) (1994) 3675.
34 T. M. MOWER and A. S. ARGON, *J. Adhes.*, to be submitted.

Received 1 June
and accepted 5 July 1994